ORIGINAL ARTICLE

OPO — THE COLLEGE OF OPTOMETRISTS

Investigating the linkage between mesopic spatial summation and variations in retinal ganglion cell density across the central visual field

Aoife M. L. Hunter[1] | **Roger S. Anderson**[1,2] | **Tony Redmond**[3] | **David F. Garway-Heath**[2] | **Pádraig J. Mulholland**[1,2]

[1]Centre for Optometry and Vision Science, Biomedical Sciences Research Institute, Ulster University, Coleraine, UK

[2]National Institute for Health Research (NIHR) Biomedical Research Centre, Moorfields Eye Hospital NHS Foundation Trust and University College London Institute of Ophthalmology, London, UK

[3]School of Optometry & Vision Sciences, Cardiff University, Cardiff, UK

Correspondence
Aoife M. L. Hunter, Centre for Optometry and Vision Science, Biomedical Sciences Research Institute, Ulster University, Coleraine, UK.
Email: a.hunter@ulster.ac.uk

Abstract

Purpose: The relationship between perimetric stimulus area and Ricco's area (RA) determines measured thresholds and the sensitivity of perimetry to retinal disease. The nature of this relationship, in addition to effect of retinal ganglion cell (RGC) number on this, is currently unknown for the adaptation conditions of mesopic microperimetry. In this study, achromatic mesopic spatial summation was measured across the central visual field to estimate RA with the number of RGCs underlying RA also being established.

Methods: Achromatic luminance thresholds were measured for six incremental spot stimuli (0.009–2.07 deg^2) and 190.4 ms duration, at four locations, each at 2.5°, 5° and 10° eccentricity in five healthy observers (mean age 61.4 years) under mesopic conditions (background 1.58 cd/m^2). RA was estimated using two-phase regression analysis with the number of RGCs underlying RA being calculated using normative histological RGC counts.

Results: Ricco's area exhibited a small but statistically insignificant increase between 2.5° and 10° eccentricity. Compared with photopic conditions, RA was larger, with the difference between RA and the Goldmann III stimulus (0.43°) being minimised. RGC number underlying RA was also higher than reported for photopic conditions (median 70 cells, IQR 36–93), with no significant difference being observed across test locations.

Conclusions: Ricco's area and the number of RGCs underlying RA do not vary significantly across the central visual field in mesopic conditions. However, RA is larger and more similar to the standard perimetric Goldmann III stimulus under mesopic compared with photopic adaptation conditions. Further work is required to determine if compensatory enlargements in RA occur in age-related macular degeneration, to establish the optimal stimulus parameters for AMD-specific microperimetry.

KEYWORDS
hill-of-vision, mesopic, microperimetry, partial summation, perimetry, Ricco's area, spatial summation

INTRODUCTION

The quantitative measurement of visual function across the central visual field with microperimetry (fundus-controlled perimetry) is fundamental to the diagnosis and monitoring of retinal diseases such as age-related macular degeneration (AMD). This test permits the measurement of contrast thresholds for a stimulus of fixed area and duration at pre-selected locations across the central visual field. Distinct from standard automated perimetry, microperimetry incorporates eye or retinal tracking such that stimulus presentations are gaze-contingent, enabling a more precise determination of visual function at defined retinal locations and a better understanding of any structure–function relationship.[1–3] In select devices, the inclusion of real-time biofeedback can also be used for eccentric fixation training in patients affected by central scotomata.[4,5] For such reasons, microperimetry is considered the reference standard visual field examination for the management of patients with unstable or eccentric fixation caused by macular pathologies.[6–9]

While microperimetry is widely accepted as a functional measure in clinical practice and as an outcome in clinical trials, it displays a number of marked limitations. These include high measurement variability,[10] a limited dynamic range[10,11] and poor sensitivity to the effects of early and intermediate AMD.[12] Previous work[13,14] has suggested that many of these limitations may be related to the design of the test and specifically the adaptation conditions used. It has been demonstrated that the sensitivity of microperimetry to early AMD and the dynamic range of the test appear to be improved by the use of mesopic rather than photopic adaptation conditions. It has been hypothesised that the ability to probe both rod- and cone-mediated function underpins the improved sensitivity of mesopic microperimetry to early AMD, where the loss of rod photoreceptors precedes cones.[15] While this theory reflects known histological changes in AMD, previous work[16] has identified the response in healthy observers to be mainly cone mediated under conventional mesopic microperimetry conditions (background luminance, 1.27 cd/m^2), with rods and cones being active in dark-adapted microperimetry (addition of a 2.0 log density filter in room illumination <0.1 lux). The principle of 'winner-takes-all' describing cone-driven suppression of rod cell activity may also contribute to the photoreceptor response in microperimetry performed under photopic, mesopic or scotopic adaptation conditions.[17] Considering this, other factors may account for the improved sensitivity of mesopic microperimetry to the effects of early AMD.

The ability of the visual system to integrate light photons over space (spatial summation) is fundamental to the detection of perimetric stimuli.[18,19] For stimuli of sufficiently small area, light energy is linearly summed by the visual system and complete spatial summation is observed, as defined by Ricco's law[20] where the product of the stimulus contrast (ΔI) and area (A), is constant at

Key points

- Unlike photopic conditions, the upper limit of complete spatial summation (Ricco's area) does not vary significantly across the central visual field in mesopic conditions.
- The number of retinal ganglion cells underlying Ricco's area in mesopic conditions was greater than for photopic conditions, but did not vary significantly across the central visual field.
- Ricco's area is closer in size to the Goldmann III stimulus in mesopic compared with photopic conditions. This likely accounts for mesopic microperimetry exhibiting improved sensitivity to age-related macular degeneration.

threshold ($\Delta I \times A = k$). The largest area for which this relationship holds is known as the area of complete spatial summation or Ricco's area (RA), with partial summation being exhibited for stimulus areas that exceed this. Other empirical laws have been proposed to describe the relationship between stimulus area and contrast thresholds where partial summation is exhibited; one such example being Piper's law[21] whereby contrast thresholds are inversely proportional to the square root of the stimulus area. The size of RA is influenced by various factors, including background illumination,[22,23] stimulus chromaticity[24] and visual field eccentricity (under photopic conditions), possibly as a noise-compensatory mechanism[25–28] such that RA contains input from a constant number of retinal ganglion cells (RGCs).[28,29] It has also been shown to change in some forms of ocular disease such as retinitis pigmentosa[30] and glaucoma.[19,31] However, we have less understanding of how RA changes in mesopic conditions, with only one study reporting spatial summation to be relatively constant with increasing visual field eccentricity in healthy observers.[32] Although in that earlier study stimuli were presented under mesopic conditions, stimulus duration was five times longer (1000 ms) than that typically used in mesopic microperimetry (200 ms), limiting clinical relevance because of the known interactions between spatial and temporal summation.[23,33]

The choice of perimetric stimulus area relative to RA has a marked influence on the sensitivity of the test to alterations in the neural architecture of the visual pathway.[19,31,34] Studies have reported the sensitivity of achromatic photopic perimetry to alterations in pathological RGC density to be improved using stimuli that are equal to, or smaller than RA such that complete spatial summation is exhibited.[19,31] Previous work has also uniformly identified the Goldmann III (GIII) stimulus to be larger than RA within the central 10° of the visual field in healthy observers under photopic conditions (10 cd/m^2), with the eccentricity at which this stimulus is equal to RA being between

10° and 20°.[26,29,34,35] It is also recognised that RA increases in size where the adapting luminance is reduced;[22,23] this likely resulting in the GIII stimulus being equal in size to RA at a more central visual field location in mesopic relative to photopic conditions. This effect is also likely exacerbated by 'filter effects' that occur secondary to outer retinal damage in conditions such as AMD,[36,37] whereby the intensity of both the stimulus and background are attenuated simultaneously to a greater extent than in healthy observers. Currently no study has quantified RA in relation to the area of GIII in mesopic compared with photopic conditions at different visual field eccentricities. Whether the number of RGCs underlying RA is a constant in mesopic adaptation conditions is also unknown. It may also be proposed that, if local spatial summation characteristics change in AMD in compensation for retinal damage (e.g., photoreceptor loss), then the damage may be more readily detected in mesopic or scotopic conditions because the conventionally used GIII stimulus equates more closely to, or is smaller than, the local RA. In this study we examined the hypothesis that the GIII stimulus more closely relates to the measured RA within the central visual field in mesopic adaptation conditions in a group of participants with no eye disease, and explored if the number of RGCs underlying RA was also constant in mesopic conditions. We also explored the effect of retinal eccentricity on partial summation, an aspect of summation that is known to vary with visual field eccentricity in photopic conditions,[35] but where no information is available for mesopic conditions.

METHODS

Participants

Five healthy observers with a mean age of 61.4 years (ages: 60 [n = 2], 61 [n = 1], 63 [n = 2]) were recruited and tested in the Centre for Optometry and Vision Science (COVS) at Ulster University, Northern Ireland. All participants had a best-corrected visual acuity of logMAR 0.0 (6/6) or better in the test eye, with spherical refractive error and astigmatism within ±6.00 and ≤1.25 D, respectively. Intraocular pressure was confirmed to be within normative limits (i.e., ≥11 and ≤21 mmHg). Slit-lamp assessment of the anterior eye and examination of the posterior segment showed no significant media opacities or ocular pathology in all participants, with optical coherence tomography (OCT) measures of peripapillary retinal nerve fibre layer thickness and macular cube (15° × 15°) within normal limits (Spectralis OCT, heidelbergengineering.com). Full visual fields were confirmed using the 24–2 SITA standard test on the Humphrey Visual Field Analyser (zeiss.com). All observers were also free of any systemic disease that may affect visual performance.

The study was reviewed and approved by the Ulster University School of Biomedical Sciences Ethics Filter Committee. The research protocol adhered to the tenets of the Declaration of Helsinki and each participant provided informed consent prior to data collection.

Apparatus and stimuli

Stimuli were generated using MATLAB (R2016b, mathworks.com) with Psychtoolbox (version 3.0), driven by a Bits# Stimulus Processor in Mono++ mode (Cambridge Research Systems, crsltd.com) and presented on a γ-corrected 21-inch cathode ray tube (CRT) display (SONY 420-GSM, sony.com; frame rate: 75 Hz, pixel resolution 1280 × 1024). A uniform background luminance of 1.58 cd/m^2 was used for all participants.[41] Chromaticity co-ordinates for the background and stimuli were $x = 0.250$ and $y = 0.295$. All luminance measurements and temporal outputs were verified with a colorimeter (ColorCAL-II; Cambridge Research Systems, crsltd.com) and Optical Transient Recorder-3 (OTR-3, Display-Messtechnik, display-messtechnik.de). Radiance measures of the display were captured using a spectroradiometer (SpecrtoCAL-MKII; Cambridge Research Systems, crsltd.com). Responses were collected using a Cedrus RB-540 response box (cedrus.com). Prior to commencing each experiment, the CRT display was allowed a minimum of 1-h warm-up time.

Achromatic luminance thresholds were measured for six incremental spot stimuli of constant duration (15 frames, 200 ms) and different area (range: –2.07 to 0.32 log deg^2) at eccentricities of 2.5°, 5° and 10°, along each of the 45°, 135°, 225° and 315° meridians. Measurements were performed for one eye only, with the test eye selected by the participant in the event of both eyes meeting the inclusion criteria. The pupil in the test eye was dilated (≥7 mm) using tropicamide hydrochloride (1%) to ensure uniform retinal illuminance in all observers. Following pupil dilation, a period of 10 min adaptation time was permitted with the participants viewing the test display in a darkened room. Refractive error for the test eye was then determined at the fovea for a viewing distance of 62 cm by an experienced optometrist. During study measurements, observers placed their heads in a secure, purpose-built chinrest while wearing a trial frame holding full-aperture corrective lenses for the test eye, and an opaque occluding patch over the fellow eye. Steady fixation on the central target was monitored visually.

Psychophysical procedure

Luminance thresholds were measured at each visual field location using a randomly interleaved 1/1 staircase and a 'Yes/No' procedure, terminating after six reversals. Stimulus area and test eccentricity were randomly selected for each test run, with each run lasting approximately 3 min. Observers were asked to press a response button to indicate stimulus detection. If no response was collected within a specified window of 2 s after stimulus presentation, then it was

registered as unseen. Stimulus luminance was decreased following a 'seen' response and increased following an 'unseen' response. Reversals in responses were registered when a change from 'seen' to 'unseen' or vice versa was detected. Stimulus luminance was changed by 0.5 log units (5 dB) up to the first reversal, by 0.25 log units (2.5 dB) up to the second reversal, by 0.1 log units (1 dB) up to the third reversal and finally by 0.05 log units (0.5 dB) for greater than three reversals. The mean of the final four reversal values was taken as the threshold at each test location. These threshold values corresponded to the 50% seen point on a psychometric function.[38] False-positive catch-trials (12 presentations, ~20% of total trial number) were also presented as 0% luminance stimuli in each test. Data were discarded if false-positive rates exceeded 20%, resulting in the participant being re-advised and that test repeated. All data were collected within a single session, lasting approximately 1.5 h for all participants. To avoid fatigue, regular rest periods were included. All participants had perimetric experience but were naïve to the protocol and completed a trial run before study measurements were performed.

Data analysis

Iterative two-phase regression analysis (Levenberg–Marquardt estimation, maximum 5000 iterations) was used to generate spatial summation functions (log threshold luminance vs. log stimulus area) and estimate RA at each test location. This analysis fits two lines to the data with the slope of the first line being constrained to −1, representing complete spatial summation in line with Ricco's law (Figure 1a). The slope and intercept of the second line in the model was free to vary, reflecting the degree of partial summation exhibited. The point at which these lines intersect, known

as the breakpoint, was taken to indicate both RA and the threshold luminance for a stimulus equal to RA. If the bilinear fit were to fail due to variability within the data set, or RA was estimated to be less than the smallest stimulus area (−2.07 log deg^2), then the data were excluded from further analysis. This analysis was undertaken for both mean data (across all observers) and at individual locations in each observer.

The effect of eccentricity on partial summation was also investigated in this study. Partial summation was quantified as the slope of the second line in each summation function, constructed using iterative two-phase regression analysis (Figure 1a). While this is the standard method to express the extent of partial summation present where a bilinear fit is used to examine summation,[39] this is limited by the fact that the transition between RA and the stimulus area where no summation is exhibited (slope = 0 for log threshold luminance vs log stimulus area) is curvilinear, this trend being described by a single linear slope value. To account for this, the mean stimulus area where summation function slope was −0.5 was identified at each location by fitting a second order polynomial function to the spatial summation data collected (log stimulus area vs. log ΔL) and examining the gradient of a tangent to this best-fitting curve at 50 uniformly spaced points between the largest and smallest stimulus areas examined (see Figure 1b). For each summation function, the mean stimulus area where the slope of the gradient to the summation function was −0.50 was identified, this analysis being repeated for each observer at all meridians and test eccentricities.

To estimate the number of RGCs underlying RA, we first estimated the average RGC density underlying stimuli. This was done using two methods in this study:

1. Histology method: To permit comparison with similar analyses undertaken in photopic conditions, we applied
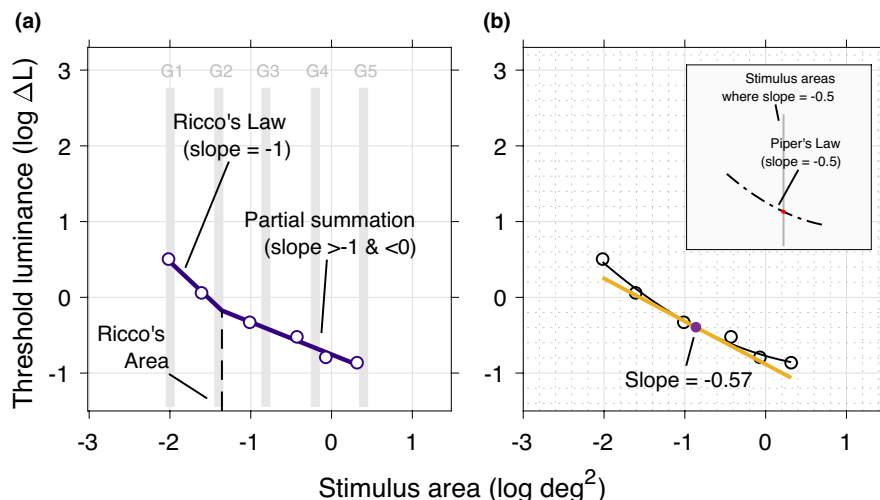

FIGURE 1 Methods used to (a) generate spatial summation functions (iterative two-phase regression analysis) and (b) examine the range of stimulus areas for which the slope of a tangent to a second order polynomial fit to the summation was −0.5 (see Methods for full description). In plot a, grey reference lines to the x-axis indicate the standardised stimulus areas; Goldmann I (G1), Goldmann II (G2), Goldmann III (G3), Goldmann IV (G4) and Goldmann V (G5).

the method proposed by Kwon and Liu.[28] In short, RGC density (all RGCs and midget RGCs) was calculated at each test location after adjustment for the lateral displacement of RGCs from underlying photoreceptors (receptive fields) using the calculation proposed by Drasdo et al.[40]

2. OCT method: We also estimated RGC density using OCT-derived retinal ganglion cell layer (RGCL) thickness measurements (from a 30°×25° posterior pole scan captured using the Spectralis OCT) and the method proposed by Raza and Hood.[41] We subsequently applied the method of Drasdo et al.,[40] incorporating the recent adjustments proposed by Montesano et al.,[42] to gain estimates of local RGC density underlying stimuli, accounting for the effect of lateral RGC displacement from underlying photoreceptors on both stimulus location and shape (where every point along the edge of the stimulus was independently displaced) at the RGC layer. In this calculation, axial length values were used to adjust the transverse scaling of OCT scans for the effect of ocular magnification, in addition to estimating stimulus area as mm^2 on the retina for each observer.

For both methods, the RGC number underlying RA was calculated as the product of stimulus area and co-localised RGC density.

The effect of increasing visual field eccentricity on RA and partial summation (summation function second line slope) was examined for each visual field meridian using a Friedman test. Post-hoc Wilcoxon signed-rank tests were used to examine pair-wise differences in RA or partial summation as indicated. An identical analysis was applied to examine the effect of visual field eccentricity on luminance thresholds measured with stimuli equal to RA (from two-phase regression analysis) and RGC number underlying RA. To examine the effect of eccentricity on the mean stimulus area where the gradient of a tangent to the summation function was −0.5, data were grouped across all meridians and observers for each eccentricity, with a Kruskal–Wallis test used to examine for statistically significant differences. For all analyses, p-values were corrected for multiple comparisons (Holm–Bonferroni correction) with an alpha (α) value <0.05 taken to be statistically significant.

RESULTS

Summary spatial summation functions for each meridian may be seen in Figure 2. An increase in RA is apparent between 2.5° and 5°, but no difference in RA measures was observed between the 5° and 10° locations. This trend is also seen when considering the individual RA estimates (Figure 2a). In total, 60 individual spatial summation functions were generated in this study. Of these, six RA estimates were excluded from further analysis due to variability in the data set (n=4) or values generated that were smaller than the minimum stimulus area (n=2).

Individual RA estimates (median, interquartile range [IQR]) were −1.29 deg^2 (IQR −1.58 to −1.14), −1.04 deg^2 (IQR −1.16 to −0.98) and −1.09 deg^2 (IQR −1.38 to −0.94), at 2.5°, 5° and 10°, respectively (Figure 2a). Differences in RA with visual field eccentricity failed to reach statistical significance for any meridian examined (45°: $\chi^2(2) = 1.5$, $p = 0.47$; 135°: $\chi^2(2) = 1.5$, $p = 0.72$; 225°: $\chi^2(5) = 1.5$, $p = 0.47$; 315°: $\chi^2(2) = 3.5$, $p = 0.17$).

Ricco's area is plotted as a function of visual field eccentricity for individual participants in each meridian (where data were available) in Figure 3. At all test locations, median RA (log deg^2) was found to be smaller than the standard GIII stimulus used in conventional microperimetry (Figure 3f). A total of 87.5%, 85% and 83.3% of RA values at 2.5°, 5° and 10° eccentricity, respectively, were smaller than the GIII stimulus.

When expressed as the slope of the second line in the summation function, the level of partial summation was found to increase as a function of eccentricity (2.5°: −0.43, IQR −0.33 to −0.46, 5°: −0.43, IQR −0.39 to −0.39, 10°: −0.55, IQR −0.41 to −0.60), but this was not statistically significant for the meridians examined (45°: $\chi^2(2) = 0.5$, $p = 0.79$; 135°: $\chi^2(2) = 4.7$, $p = 0.10$; 225°: $\chi^2(5) = 1.5$, $p = 0.47$; 315°: $\chi^2(2) = 2.0$, $p = 0.34$, Figure 4a). In similar fashion, we also observed that the median stimulus area (log deg^2) for which the slope of a tangent to the summation function was −0.5 varied with eccentricity (2.5°: −0.53, IQR −0.77 to −0.35, 5°: −0.41, IQR −0.58 to −0.03, 10°: −0.12, IQR −0.27 to 0.05); these differences were statistically significant for all meridians examined (45°: $\chi^2(2) = 16.9$, $p < 0.001$; 135°: $\chi^2(2) = 19.0$, $p < 0.001$; 225°: $\chi^2(5) = 6.3$, $p = 0.04$; 315°: $\chi^2(2) = 22.5$, $p = 0.001$, Figure 4b). Post-hoc tests revealed statistically significant differences in the median stimulus areas for which the slope of the tangent to the summation function was −0.5 at 2.5° and 10° eccentricities along the 45°, 135° and 315° meridians (all $p < 0.001$). Statistically significant differences were also observed between locations at 2.5° and 5° along the 45° and 315° meridians (both $p < 0.001$), in addition to locations at 5° and 10° along the 45° meridian ($p = 0.001$).

In line with previous studies undertaken in photopic adaptation conditions,[27,39] luminance at threshold (log ΔL) for stimuli equal to RA were similar for locations at 2.5° (−0.23, IQR −0.21 to −0.12) and 5° eccentricity (−0.23, IQR −0.31 to −0.14). However, luminance thresholds for a stimulus equal to RA were higher for locations at 10° eccentricity (0.20, IQR −0.11 to 0.49) compared with 2.5° and 5° eccentricities. These differences were not statistically significant for any meridians examined (all $p > 0.05$; Figure S1).

The number of RGCs (all cell types) found to underlie RA was relatively constant between visual field locations at 2.5° (83.0 cells, IQR 39.7–114.0) and 5° (90.0 cells, IQR 62.6–102.6), but lower at 10° (27.6 cells, IQR 11.0–45.1) when estimated using normative histological data. These trends were also replicated for midget RGCs (2.5°: 66.6 cells, IQR 31.8–91.5; 5°: 69.4 cells, IQR 48.3–79.3; 10°: 19.2 cells, IQR 7.6–31.3). Very similar trends were also observed when RGC number (all subtypes) underlying RA was estimated using
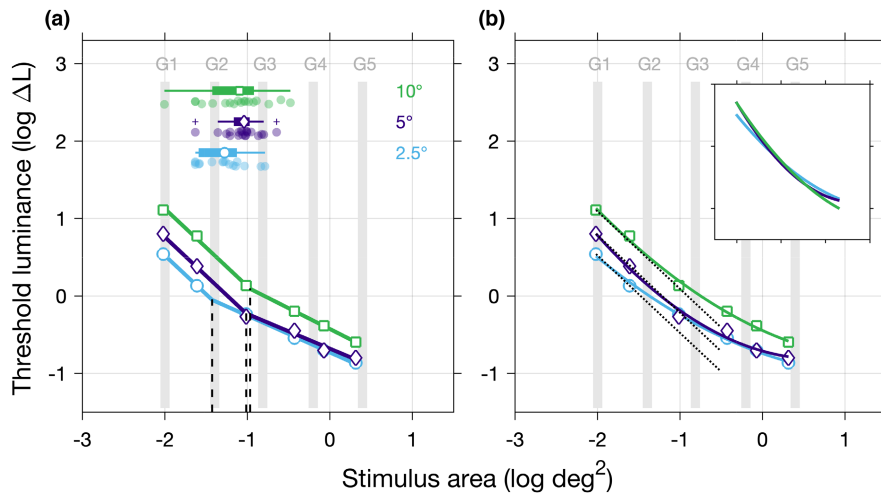
FIGURE 2 Mean spatial summation functions at each test eccentricity (2.5–10°) constructed using (a) iterative two-phase regression analysis and (b) a second-order polynomial function. Grey reference lines to the x-axis indicate the standardised Goldmann stimulus areas (G1–G5) used in perimetry. In plot a, the dashed lines to the x-axis represent the estimated Ricco's area (RA) values, with boxplots of RA measures in individual observers also being included for reference. In plot b, a reference line of −1 slope (indicating complete summation, dotted line) is included, with the inset plot including a vertical translation of the summation functions (to account for luminance threshold differences with eccentricity) for comparison.

participant specific OCT scans (Figure 5c; 2.5°: 105.9 cells, IQR 58.5–176.1; 5°: 127.8 cells, IQR 100.4–165.6; 10°: 46.0 cells, IQR 20.9–68.1). Despite such differences, no statistically significant change in the number of RGCs underlying RA was observed with eccentricity (45°: $\chi^2(2) = 3.5$, $p = 0.35$; 135°: $\chi^2(2) = 4.7$, $p = 0.29$; 225°: $\chi^2(5) = 1.5$, $p = 0.47$; 315°: $\chi^2(2) = 6.5$, $p = 0.16$).

DISCUSSION

In this study, we examined spatial summation across the central visual field (2.5–10°) in mesopic adaptation conditions. RA was found to be larger in mesopic compared with previously reported values for photopic conditions,[28,35] in addition to being more similar in size to the standard GIII perimetric stimulus in mesopic conditions. No statistically significant change in RA across the central visual field was observed, with any differences being smaller than those seen in photopic conditions across the same visual field eccentricities.[28,43] Incomplete or partial summation, expressed as the slope of the second component line in each spatial summation function constructed, increased with visual field eccentricity, but this change failed to reach statistical significance. In contrast, the median interpolated stimulus size where the tangent to the summation function slope was −0.5 was significantly larger at 10° compared with 2.5°. No statistically significant variation in RGC number underlying RA was found across the retinal locations examined.

While it is universally reported that RA enlarges as a function of visual field eccentricity in photopic conditions,[26–28,44] only one previous study[32] examined spatial summation across the central visual field in mesopic

adaptation conditions. In agreement with the findings of the current investigation (Figure 2b), Dannheim and Drance[32] reported the shape of spatial summation functions collected in mesopic conditions, for a stimulus duration of 1 s, to remain constant between 0° and 30° eccentricity along the 45° meridian in healthy participants aged 20–79 years. Conversely, spatial summation function shape was found to alter markedly between the same visual field locations in photopic conditions (background 3.18 cd/m²). Despite such trends, the authors reported that the maximal change in stimulus diameter (from 0.083° to 2°) induced a change in contrast thresholds that was approximately 40% greater at 30° compared with 5° eccentricity under both mesopic and photopic adaptation conditions. A similar observation was made in the current study whereby changing stimulus area from 0.01 to 2.07 deg² induced a 30.3% greater change in thresholds at 10° compared with 2.5° eccentricity. In the absence of alterations in RA, it is likely such findings may be accounted for by an increased degree of partial summation at 10° compared with 2.5°; this trend being observed in this study (Figure 4). Using similar methodology, Choi et al.[35] reported partial summation to increase with visual field eccentricity under photopic conditions, the extent of partial summation being lower compared with those in the current study. An alternative explanation is that changes in complete spatial summation, although present, were small and potentially may not have reached statistical significance in view of this (Figure 3f).

Changes in photopic spatial summation with visual field eccentricity have been hypothesised to be a noise compensatory mechanism strongly related to local RGC density, whereby a critical number of functionally intact RGCs underlie RA.[28,29] Swanson et al.[29] demonstrated the relationship between the number of RGCs underlying a
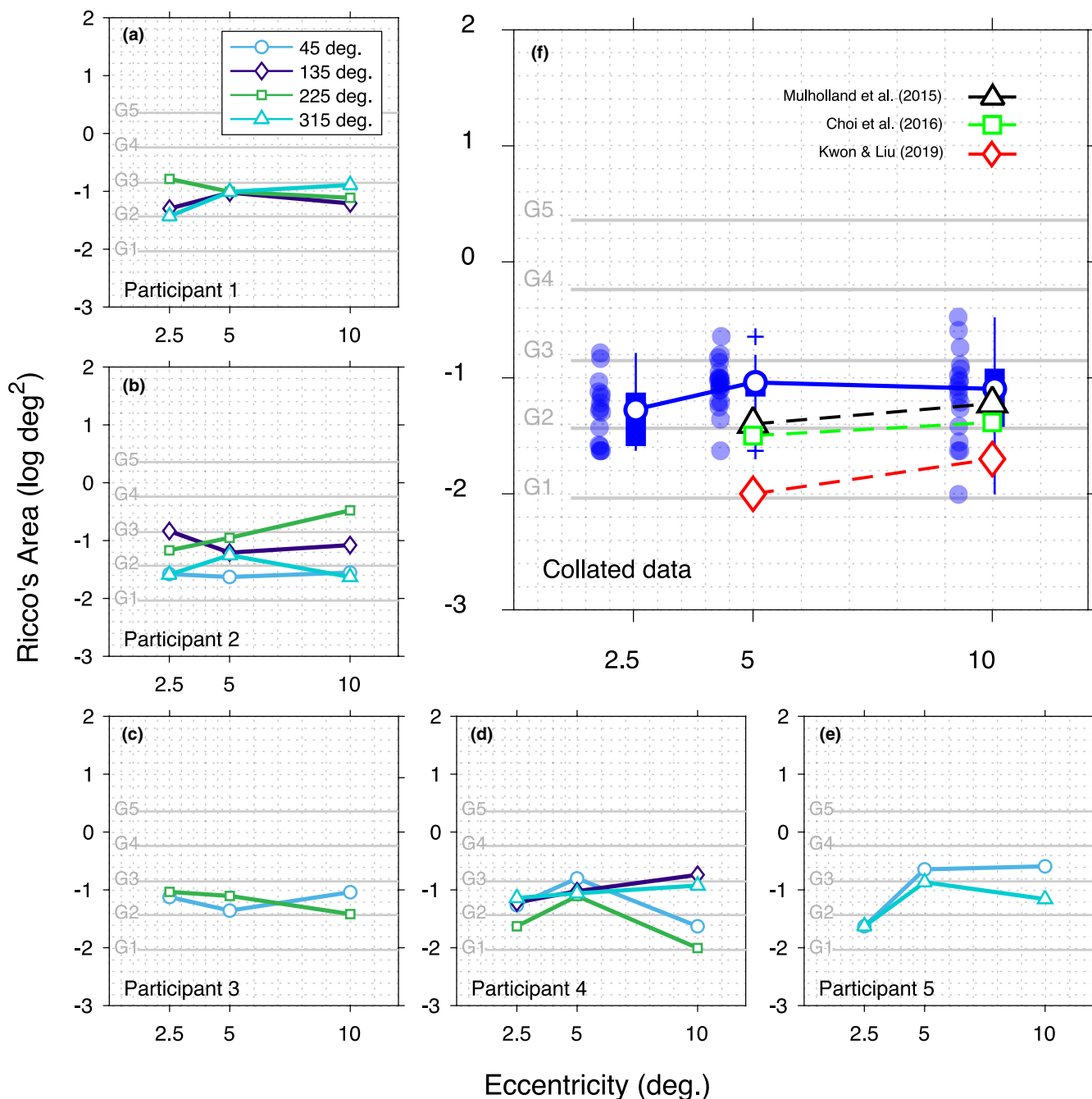
FIGURE 3   Changes in Ricco's area (RA) with visual field eccentricity for individual participants (a–e) and all participants and locations (f). Meridians were omitted from plots where RA values computed for one or more test locations were excluded. Comparisons with studies undertaken in photopic conditions are included for reference in (f). Grey reference lines to the y-axis indicate the area of Goldmann stimuli I to V (G1–G5).

GIII stimulus (estimated from normative histological RGC counts[45]) and photopic contrast thresholds for the same stimulus to be best described by a two-phase linear model whereby a slope of unity was observed when the RGC number was ≤31.6 cells (~15° eccentricity); this broke down when the cell number was >31.6 (0–15° eccentricity). More recently, RA was found to enlarge between 4° and 18.5° eccentricity, with the number of RGCs underlying RA reported to be constant (~14 RGCs), accounting for 89% of the variance in RA with eccentricity, with the same number of RGCs determining contrast detection when calculated

using a retina-V1 model.[28] Interestingly, a lower, but still constant number of midget RGCs (~10) were estimated to underlie RA; this accounted for a comparatively lower 79% of the variance in RA with eccentricity. While such evidence points strongly to RGC number determining the extent of RA and its variation across the visual field in photopic conditions, such trends were not observed in the current study whereby only 49.2% of the variance in RA with eccentricity was explained by variations in overall RGC density (calculated using methods proposed by Kwon and Liu[28]). Furthermore, the difference in the contribution of
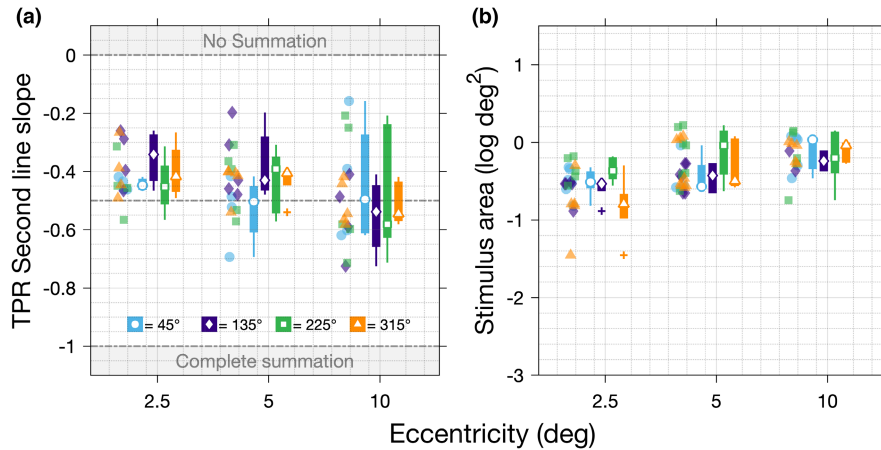
FIGURE 4 Boxplots of (a) iterative two-phase regression (TPR) second line slope (representing partial summation) for each meridian examined at all test eccentricities (included for reference are dashed lines at 0, 0.5 and 1 to represent the slope when summation is totally absent, Piper's law applies or complete summation is present) and (b) the range of stimulus areas where the slope of a tangent to the summation function was −0.5 at each test eccentricity.
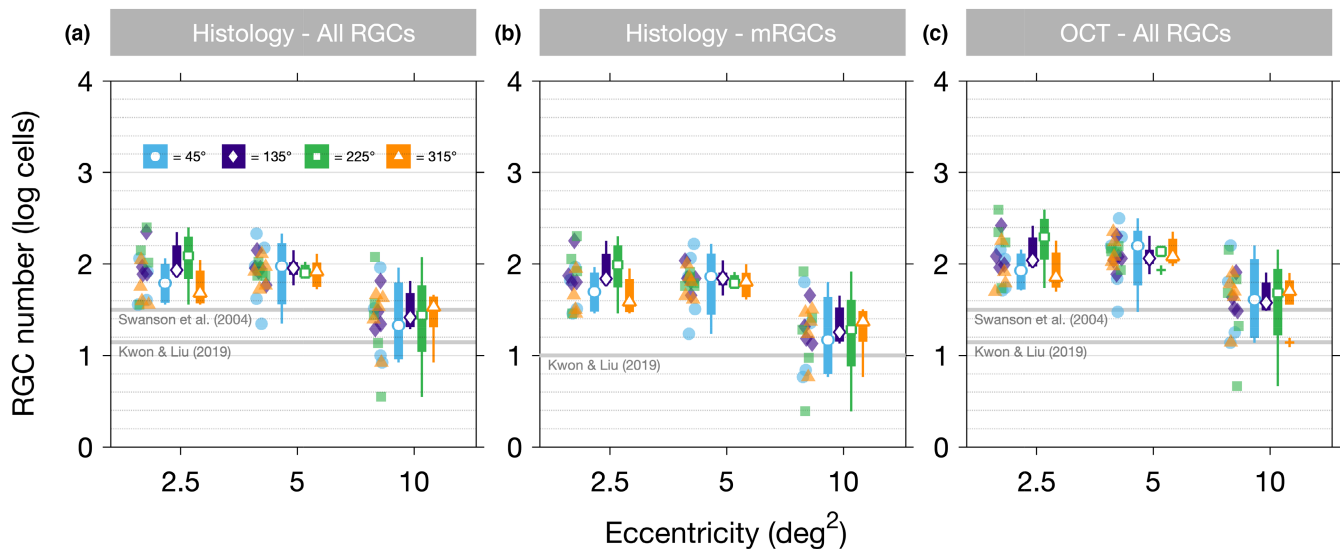

FIGURE 5 Boxplots of retinal ganglion cell (RGC) number underlying Ricco's area (RA) calculated using mean histology (all subtypes [a] and midget cells [b]) and (c) macular optical coherence tomography (OCT) scans for each visual field eccentricity examined in mesopic conditions. Included for reference are the number of cells reported to underlie RA in photopic conditions (solid grey lines).

midget RGCs to RA changes (52.4%) compared with all RGC subtypes (49.2%), was found to be smaller than reported in photopic conditions.

Unsurprisingly, the size of RA, and thus, the number of RGCs found to underlie a stimulus equal to RA at each eccentricity appears to be higher than those reported in photopic conditions.[28,29] These findings likely reflect dynamic alterations in the organisation of antagonistic centre-surround RGC receptive fields, a feature hypothesised to contribute at least in part to determining the extent of RA at a given location. Evidence for altered RGC receptive field characteristics with adaption conditions may be seen in the work of Barlow et al.[46] In that study, ex vivo recordings of cat RGCs revealed the inhibitory surround of centre-surround antagonistic RGC receptive

fields to be negligible with some enlargement of the centre following a period of dark-adaptation; these changes were attributed to reduced lateral inhibition in the dark-adapted retina. Wiesel and Hubel[47] observed a similar trend for receptive fields of parvocellular cells at threshold in the lateral geniculate nucleus of macaque monkeys. Psychophysical evidence for reduced inhibitory surround size following dark adaptation in human observers may also be inferred from pattern-evoked electroretinograms undertaken in light- and dark-adapted conditions.[48] However, no such changes in basic receptive field characteristics have been reported in V1 of the monkey visual cortex.[49] Additionally, contrast sensitivity (area under the log contrast sensitivity function and peak log contrast sensitivity) is lower in older (compared with

younger) adults under mesopic versus photopic adaptation conditions,[50] which may also contribute to the enlargement in RA in mesopic conditions.

While an increase in RA in mesopic relative to photopic conditions was anticipated, it appears that the number of RGCs underlying RA is not constant across all locations examined here (Figure 5). This contrasts with photopic conditions where the RGC number underlying RA is essentially constant at all locations.[28] Considering such trends, it is possible that alterations in receptive field characteristics at the retina and/or visual cortex, rather than RGC density alone, may account for the observed lack of uniformity in RGC number in RA. Previous work in the primate retina has identified differences in receptive field areas between RGC types, with magnocellular (parasol) RGCs displaying larger receptive field areas compared with parvocellular (midget) RGCs, with such differences contributing to an increased linear response to contrast changes (higher contrast gain) and prolonged functioning in lower adapting luminances.[51] Considering the ratio of midget RGCs to other RGC subtypes alters markedly from the fovea to mid-peripheral retina.[52] Thus, any relative variation in receptive field organisation with visual field location may lead to differences in the nature of any changes in RA and thus RGC number underlying a RA stimulus under non-photopic adapting luminances. An alternative explanation may be that RGC number at RA is not constant at all locations in the visual field, as previously hypothesised. Closer examination of the data presented by Kwon and Liu[28] for photopic conditions reveals the RGC number at RA to be higher in the central visual field, with the RGC number being relatively constant for locations beyond 8° eccentricity. The trend towards higher RGC counts at 2.5° and 5° eccentricities (Figure 5) compared with 10° was also replicated in the present study where both average histology and participant specific OCT data were used to generate estimates of RGC density. However, this trend may reflect the fact that parasol cells most likely mediate responses to the stimuli presented. It has previously being reported in primate work that parasol cells are preferentially stimulated by perimetric stimuli.[51,53]

The results of this study also indicate that the GIII stimulus conventionally used in microperimetry is markedly closer in size to RA in the central 10° of the visual field in mesopic compared with photopic conditions (Figure 3f).[28] This is significant considering our observation that the slope of the hill-of-vision, and thus, sensitivity to changes in the density of photoreceptors and RGCs across the retina, is markedly influenced by stimulus area and the extent of spatial summation that is exhibited. The slope of the hill-of-vision appears to reduce proportionally to the degree of summation exhibited, this being highest for stimuli exhibiting complete spatial summation (Figure S1a,b) with a small decline for increases in stimulus area over which partial summation is present (Figure S1c–f).[39]

As the GIII stimulus in photopic conditions is markedly larger than RA within the central 10° of the visual field, it may be argued that the stimulus will be insensitive to small changes in the neural architecture of the retina in conditions such as AMD. In contrast, it may be hypothesised that the use of the same stimulus in mesopic conditions, where RA is closer in size to the GIII stimulus, will permit more subtle variations in disease status to be detected, thus somewhat accounting for the improved sensitivity of mesopic relative to photopic microperimetry.[6,54,55] Furthermore, should spatial summation be altered as part of the AMD disease process, then such changes would be more readily detected in mesopic conditions owing to the smaller differences between the GIII stimulus and local RA measures. Such changes in spatial summation may be underpinned by a 'filter effect' that has been demonstrated in photoreceptor disorders whereby cone function (and thus measured sensitivity) is affected when assessed in mesopic conditions.[36,37] These effects have been highlighted in threshold vs. intensity (tvi) curves, with conditions where receptoral damage was present leading to an upwards and rightwards shift[36,56] of the tvi curve relative to control data. While it is acknowledged that spatial vision is impaired in AMD, previous work has suggested that RA is unchanged as part of the disease process.[57] Importantly, no study has investigated this under standardised microperimetry conditions where stimulus presentations are gaze-contingent. Such work is essential to determine the optimal stimulus characteristics for use in an AMD-specific perimetric test of visual function.

CONCLUSIONS

The area of complete spatial summation (RA) is smaller than a standard GIII stimulus and varies insignificantly across the central visual field examined in this study, under adaptation conditions of mesopic microperimetry. This is in contrast to photopic conditions where RA increases as a function of visual field eccentricity, with the GIII stimulus also being markedly larger than RA in the central visual field. Further work is required to determine if compensatory enlargements in RA occur in varying degrees of macular disease such as AMD, increasingly examined by microperimetry. This may have implications for the selection of the optimal stimuli for use in microperimetry.

AUTHOR CONTRIBUTIONS
Aoife M. L. Hunter: Conceptualization (supporting); data curation (lead); formal analysis (equal); investigation (lead); methodology (supporting); project administration (equal); resources (supporting); software (supporting); validation (supporting); visualization (equal); writing – original draft (lead); writing – review and editing (equal). **Roger S. Anderson:** Conceptualization (supporting); funding acquisition (supporting); investigation (supporting); methodology (supporting); project administration (supporting); resources (supporting); software (supporting);

CONFLICT OF INTEREST STATEMENT

A.M.L. Hunter, None; R.S. Anderson, Visual field sensitivity testing (P), Alliance Pharmaceutical (R); T. Redmond, Visual field sensitivity testing (P); D.F. Garway-Heath, Visual field sensitivity testing (P), Alcon Research Institute (F), Janssen (F, C), Santen (F, C), Novartis (F), CenterVue (R, C), Heidelberg Engineering (R), Oculus (R), Topcon (R), Allergan (C), Bausch-Lomb (C), Genentech (C), Omikron (C), Roche (C); P.J. Mulholland, Visual field sensitivity testing (P), Heidelberg Engineering Gmbh (F), LKC Inc. (F).

ORCID

Aoife M. L. Hunter https://orcid.org/0000-0002-0150-4126

Tony Redmond https://orcid.org/0000-0002-6997-5231

REFERENCES

1. Inatomi A. A simple fundus perimetry with fundus camera. In: Greve EL, editor. Documenta Ophthalmologica proceedings series. Volume 19. The Hague: Dr W. Junk b. v. Publishers; 1979. p. 359–62.
2. Markowitz SN, Reyes SV. Microperimetry and clinical practice: an evidence-based review. *Can J Ophthalmol*. 2013;48:350–7.
3. Martín AM, Piñero DP, Pérez-Cambrodí RJ. Normal values for microperimetry with the MAIA microperimeter: sensitivity and fixation analysis in healthy adults and children. *Eur J Ophthalmol*. 2017;27:607–13.
4. Nidek Technologies Srl. MP-1 microperimeter. Padova: Nidek Co., Ltd.; 2013. p. 1–4.
5. Centrevue. Macular integrity assessment (MAIA) handbook. Padova: Centrevue; 2013. p. 1–29.
6. Rohrschneider K, Bültmann S, Springer C. Use of fundus perimetry (microperimetry) to quantify macular sensitivity. *Prog Retin Eye Res*. 2008;27:536–48.
7. Acton JH, Greenstein VC. Fundus-driven perimetry (microperimetry) compared to conventional static automated perimetry: similarities, differences, and clinical applications. *Can J Ophthalmol*. 2013;48:358–63.
8. Liu H, Bittencourt MG, Wang J, Sepah YJ, Ibrahim-Ahmed M, Rentiya Z, et al. Retinal sensitivity is a valuable complementary measurement to visual acuity—a microperimetry study in patients with maculopathies. *Graefes Arch Clin Exp Ophthalmol*. 2015;253:2137–42.
9. Chiang WY, Lee JJ, Chen YH, Chen CH, Chen YJ, Wu PC, et al. Fixation behavior in macular dystrophy assessed by microperimetry. *Graefes Arch Clin Exp Ophthalmol*. 2018;256:1403–10.
10. Chen FK, Patel PJ, Xing W, Bunce C, Egan C, Tufail AT, et al. Test–retest variability of microperimetry using the Nidek MP1 in patients with macular disease. *Invest Ophthalmol Vis Sci*. 2009;50:3464–72.
11. Steinberg JS, Saßmannshausen M, Pfau M, Fleckenstein M, Finger RP, Holz FG, et al. Evaluation of two systems for fundus-controlled scotopic and mesopic perimetry in eye with age-related macular degeneration. *Transl Vis Sci Technol*. 2017;6:7. https://doi.org/10.1167/tvst.6.4.7
12. Maynard ML, Zele AJ, Feigl B. Mesopic Pelli–Robson contrast sensitivity and MP-1 microperimetry in healthy ageing and age-related macular degeneration. *Acta Ophthalmol*. 2016;94:e772–8.
13. Sunness JS, Rubin GS, Broman A, Applegate CA, Bressler NM, Hawkins BS. Low luminance visual dysfunction as a predictor of subsequent visual acuity loss from geographic atrophy in age-related macular degeneration. *Ophthalmology*. 2008;115:1480–8.
14. Owsley C, Huisingh C, Clark ME, Jackson GR, Mcgwin G. Comparison of visual function in older eyes in the earliest stages of age-related macular degeneration to those in normal macular health. *Curr Eye Res*. 2016;41:266–72.
15. Curcio CA, Medeiros NE, Millican CL. Photoreceptor loss in age-related macular degeneration. *Invest Ophthalmol Vis Sci*. 1996;37:1236–49.
16. Simunovic MP, Moore AT, MacLaren RE. Selective automated perimetry under photopic, mesopic, and scotopic conditions: detection mechanisms and testing strategies. *Transl Vis Sci Technol*. 2016;5:10. https://doi.org/10.1167/tvst.5.3.10
17. Lauritzen JS, Sigulinsky CL, Anderson JR, Kalloniatis M, Nelson NT, Emrich DP, et al. Rod-cone crossover connectome of mammalian bipolar cells. *J Comp Neurol*. 2019;527:87–116.
18. Anderson RS. The psychophysics of glaucoma: improving the structure/function relationship. *Prog Retin Eye Res*. 2006;25:79–97.
19. Redmond T, Garway-Heath DF, Zlatkova MB, Anderson RS. Sensitivity loss in early glaucoma can be mapped to an enlargement of the area of complete spatial summation. *Invest Ophthalmol Vis Sci*. 2010;51:6540–8.
20. Ricco A. Relazione fra il minimo angolo visuale e l'intensità luminosa. *Memorie R Accad Sci Lett Modena*. 1877;17:47–160.
21. Piper H. Über die Abhängigkeit des Reizwertes leuchtender Objekte von ihre Flachen-bezw. *Winkelgrasse Z Psychol Physiol Sinnesorgane*. 1903;32:98–112.
22. Redmond T, Zlatkova MB, Vassilev A, Garway-Heath DF, Anderson RS. Changes in Ricco's area with background luminance in the S-cone pathway. *Optom Vis Sci*. 2013;90:66–74.
23. Barlow HB. Temporal and spatial summation in human vision at different background intensities. *J Physiol*. 1958;141:337–50.
24. Volbrecht VJ, Shrago EE, Schefrin BE, Werner JS. Ricco's areas for S- and L-cone mechanisms across the retina. *Color Res Appl*. 2000;26:S32–5.

25. Volbrecht VJ, Shrago EE, Schefrin BE, Werner JS. Spatial summation in human cone mechanisms from 0° to 20° in the superior retina. *J Opt Soc Am*. 2000;17:641–50.

26. Khuu SK, Kalloniatis M. Spatial summation across the central visual field: implications for visual field testing. *J Vis*. 2015;15:15.1.6. https://doi.org/10.1167/15.1.6

27. Wilson ME. Invariant features of spatial summation with changing locus in the visual field. *J Physiol*. 1970;207:611–22.

28. Kwon MY, Liu R. Linkage between retinal ganglion cell density and the nonuniform spatial integration across the visual field. *Proc Natl Acad Sci USA*. 2019;116:3827–36.

29. Swanson WH, Felius J, Pan F. Perimetric defects and ganglion cell damage: interpreting linear relations using a two-stage neural model. *Invest Ophthalmol Vis Sci*. 2004;45:466–72.

30. Swanson WH, Felius J, Birch DG. Effect of stimulus size on static visual fields in patients with retinitis pigmentosa. *Ophthalmology*. 2000;107:1950–4.

31. Mulholland PJ, Redmond T, Garway-Heath DF, Zlatkova MB, Anderson RS. Spatiotemporal summation of perimetric stimuli in early glaucoma. *Invest Ophthalmol Vis Sci*. 2015;56:6473–82.

32. Dannheim F, Drance SM. Studies of spatial summation of central retinal areas in normal people of all ages. *Can J Ophthalmol*. 1971;6:311–9.

33. Owen WG. Spatio-temporal integration in the human peripheral retina. *Vision Res*. 1972;12:1011–26.

34. Rountree L, Mulholland PJ, Anderson RS, Garway-Heath DF, Morgan JE, Redmond T. Optimising the glaucoma signal/noise ratio by mapping changes in spatial summation with area-modulated perimetric stimuli. *Sci Rep*. 2018;8:2172. https://doi.org/10.1038/s41598-018-20480-4

35. Choi AYJ, Nivison-Smith L, Khuu SK, Kalloniatis M. Determining spatial summation and its effect on contrast sensitivity across the central 20 degrees of visual field. *PLoS One*. 2016;11:e158263. https://doi.org/10.1371/journal.pone.0158263

36. Hood DC, Greenstein V. Models of the normal and abnormal rod system. *Vision Res*. 1990;30:51–68.

37. Simunovic MP, Hess K, Avery N, Mammo Z. Threshold versus intensity functions in two-colour automated perimetry. *Ophthalmic Physiol Opt*. 2021;41:157–64.

38. Levitt H. Transformed up-down methods in psychoacoustics. *J Acoust Soc Am*. 1971;49:467–77.

39. Khuu SK, Kalloniatis M. Standard automated perimetry: determining spatial summation and its effect on contrast sensitivity across the visual field. *Invest Ophthalmol Vis Sci*. 2015;56:3565–76.

40. Drasdo N, Millican CL, Katholi CR, Curcio CA. The length of Henle fibers in the human retina and a model of ganglion receptive field density in the visual field. *Vision Res*. 2007;47:2901–11.

41. Raza AS, Hood DC. Evaluation of the structure-function relationship in glaucoma using a novel method for estimating the number of retinal ganglion cells in the human retina. *Invest Ophthalmol Vis Sci*. 2015;56:5548–56.

42. Montesano G, Ometto G, Hogg RE, Rossetti LM, Garway-Heath DF, Crabb DP. Revisiting the Drasdo model: implications for structure–function analysis of the macular region. *Transl Vis Sci Technol*. 2020;9:15. https://doi.org/10.1167/tvst.9.10.15

43. Mulholland P, Redmond T, Zlatkova M, Garway-Heath D, Anderson R. Temporal summation varies with visual field eccentricity for perimetric stimuli scaled to the area of complete spatial summation. *Invest Ophthalmol Vis Sci*. 2013;15:ARVO E-Abstract 3924.

44. Inui T, Mimura O, Kani K. Retinal sensitivity and spatial summation in the foveal and parafoveal regions. *J Opt Soc Am*. 1981;71:151–63.

45. Curcio CA, Allen KA. Topography of ganglion cells in human retina. *J Comp Neurol*. 1990;300:5–25.

46. Barlow HB, Fitzhugh R, Kuffler SW. Change of organization in the receptive fields of the cat's retina during dark adaptation. *J Physiol*. 1957;137:338–54.

47. Wiesel TN, Hubel DH. Spatial and chromatic interactions in the lateral geniculate body of the rhesus monkey. *J Neurophysiol*. 1966;29:1115–56.

48. Korth M, Ilschner S, Sembritzki O. Retinal receptive fields under different adaptation levels studied with pattern-evoked ERG. *Graefes Arch Clin Exp Ophthalmol*. 1987;225:63–9.

49. Duffy KR, Hubel DH. Receptive field properties of neurons in the primary visual cortex under photopic and scotopic lighting conditions. *Vision Res*. 2007;47:2569–74.

50. Owsley C, Swain T, Liu R, McGwin G, Kwon MY. Association of photopic and mesopic contrast sensitivity in older drivers with risk of motor vehicle collision using naturalistic driving data. *BMC Ophthalmol*. 2020;20:47. https://doi.org/10.1186/s12886-020-1331-7

51. Kaplan E, Lee BB, Shapley RM. Chapter 7 New views of primate retinal function. *Prog Ret Res*. 1990;9:273–336.

52. Dacey DM. The mosaic of midget ganglion cells in the human retina. *J Neurosci*. 1993;13:5334–55.

53. Swanson WH, Sun H, Lee BB, Cao D. Responses of primate retinal ganglion cells to perimetric stimuli preparation for ganglion cell recordings. *Invest Ophthalmol Vis Sci*. 2011;52:764–71.

54. Feigl B, Brown B, Lovie-Kitchin J, Swann P. Monitoring retinal function in early age-related maculopathy: visual performance after 1 year. *Eye*. 2005;19:1169–77.

55. Hogg RE, Chakravarthy U. Visual function and dysfunction in early and late age-related maculopathy. *Prog Retin Eye Res*. 2006;25:249–76.

56. Kalloniatis M, Harwerth RS, Smith EL, DeSantis L. Colour vision anomalies following experimental glaucoma in monkeys. *Ophthalmic Physiol Opt*. 1993;13:56–67.

57. Zele AJ, O'Loughlin RK, Guymer RH, Vingrys AJ. Disclosing disease mechanisms with a spatio-temporal summation paradigm. *Graefes Arch Clin Exp Ophthalmol*. 2006;244:425–32.

SUPPORTING INFORMATION

Additional supporting information can be found online in the Supporting Information section at the end of this article.